Enhanced subsurface investigation utilizing electrical resistivity tomography and precise positioning tools (study case: Rongga landslide)

Moch Hilmi Zaenal Putra[1*], *Adrin* Tohari[1], *Eko* Soebowo[1], *Yayat* Sudrajat[1], *Amar*[1], *Wahyudin*[1], and *Dadan Dani* Wardhana[1]

[1]Geological Disaster Research Center, National Research and Innovation Agency, Bandung, Indonesia

Abstract. This study presents an enhanced approach for subsurface investigation using Electrical Resistivity Tomography (ERT) coupled with precise positioning tools, focusing on the Rongga Landslide in Indonesia. ERT is widely recognized for its ability to map subsurface conditions by detecting resistivity contrasts associated with geological structures and water content, especially in landslide-prone areas. The study combines GPS and digital waterpass altimeter with ERT to improve the precision of subsurface anomaly detection. Important information regarding moisture distribution, graben structures, and sliding surfaces was revealed by the generation of two ERT profiles. Our research indicates that a number of factors, including lithological characteristics, erosion along riverbanks, and tectonic activity—specifically, a nearby fault structure—may have contributed to the Rongga landslide These findings highlight the usefulness of ERT to evaluate the risk of landslides and offer useful data for geotechnical research in tectonically active areas.

1 Introduction

Recent research evidences the potential of Electrical Resistivity Tomography (ERT) as a predictor of landslides in volcanic areas. For instance, the use of ERT in landslide studies, showing how the application can be useful and its limitations in sector analysis [1]. ERT was most effective in reconstructing the slope geometry, locating the sliding surface as well as in mapping the high-water content areas. Some insights on the use of ERT in landslides, as a special case, the Lijiazu landslide in Hunan province was investigated in terms of it [2]. It is good for its mobilization flexibility and adaptability in different regions including areas with mountainous terrain. The approach enables determination of the landslide sliding surface, thickness and altitude, providing an effective means for understanding of the deformation and failure process of landslides. Application of the ERT method for characterizing landslides in Southwest China [3]. Units under assessment are units that are at higher risk for landslides. This research is about understanding what happened in the subsurface before the landslide. The ERT surveys consisted of two merged profiles that were designed to reveal patterns related to movement on the landslide mass and manner of the sliding surface and bedrock geoelectrical properties. The low resistivity of the sliding parts, corresponding to weathered sandstone and mudstone layers, was a major result. The research demonstrates the potential benefit of using ERT to detect subsurface conditions crucial for landslide hazard assessment and mitigation.

ERT is a powerful and informative technique to predict landslides in volcanic areas since it allows detailed subsurface imaging and can detect slight differences in water content [4]. False interpretations may occur due to soil type, moisture content, temperature, electrode contact, survey configuration and surface conditions, which might lower the reliability and accuracy of ERT measurements.

1.1 Geology

The study area is situated in the mountainous region at an average elevation of 1,000 meters above the sea level. This area overlies with Tertiary formations consisting of Mts, Mtb, Tmc, Tmcs, and Tmbe (Fig. 1a) [5]. The regions geodynamic history favored the presence of various structural features including anticlines, normal faults, and strike-slip faults [5].

Toe parts of the landslide area are located near to the riverbank of Cidadap River, which belong to Tmc formation specifically. The Tmc unit consists of interbedded claystone, siltstone, and sandstone, and local lahar beds of tuff, andesite breccia, and tuff breccia. The mountainous topography and the structural intricacies within the Tmc formation together with its geological properties, make this area landslide-prone.

The landslide area is located at a geological structure of anticline with folded lithology and the anticline is

* Corresponding author : mochhilmizp@gmail.com

oriented southeast - northwest. An anticline observed in the Tmc formation following active calls to the tectonics of the compression, suggested that this anticline formation occurred after the Middle Miocene.

Field mapping results and measurements were put together to generate the lithological variations within the landslide area. The slope bottom portion is occupied with sedimentary siltstone and sandstone horizons (Fig. 1b). Above the sedimentary this layer is then topped with a tuff layer; which is an indication of previous volcanic activity (Fig. 1c). Top of slope: a thick, weathered volcanic soil. The bare soil of the main landslide body is about four meters thick at its top of scarp, the upper part being red brown and the lower dark brown. These colors represent weathered procedures.

It is a process of weathering we can see the progression in soil profile. The reddish-brown colouration of the upper part of the volcanic soil layer shown below suggests oxidation and iron oxides which are characteristic of prolonged exposure to the atmosphere. This is a reflection of abundant exposure of the soils to the surface and therefore a lot of time for chemical weathering to take place. Conversely, the dark brown color of the lower part of the soil layer potentially involves less oxidation and overall organic matter would be higher. This weathering has led to such distinct soil horizons as to mirror the history of the stability and exposure of the land surface.

The fact that the weathered soil layers are present displaying different colorations and characteristics indicates that the soil is existing on the surface from a long period during which it has undergone the process of weathering widely. While the long-term exposure has allowed the evidence of a mature soil history to develop, and thereby emphasizing the intricate and dynamic interaction between geological processes and more recent environmental conditions.

The outcrop showcases a cornucopia of structures that provide clues to the environmental changes that affected this region. Essentially, strata represent phases or periods of depositional processes influenced by different forces, most likely rivers, lakes and marine environments that have left different marks or layers in the sediments over time. These tuffs gave enormous evidence of active volcanism during the Tertiary period, just above these compound sedimentary layers. External to these geological remnants a weathered volcanic profile soils its way to a landscape having been stable and exposed for millennium. This specific soil profile reflects a period of time when material was weathered chemically, and also when the structure began to be broken up physically, leading mature soil structure to form on a stationary land surface.

The features combine to form a multifaceted geological story about eruptions of volcanoes interspersed with silty periods of erosion and ash soil creation. The complex tale that is told tracks the changing face of the landscape from Middle Miocene through to modern day, at a geological scale.

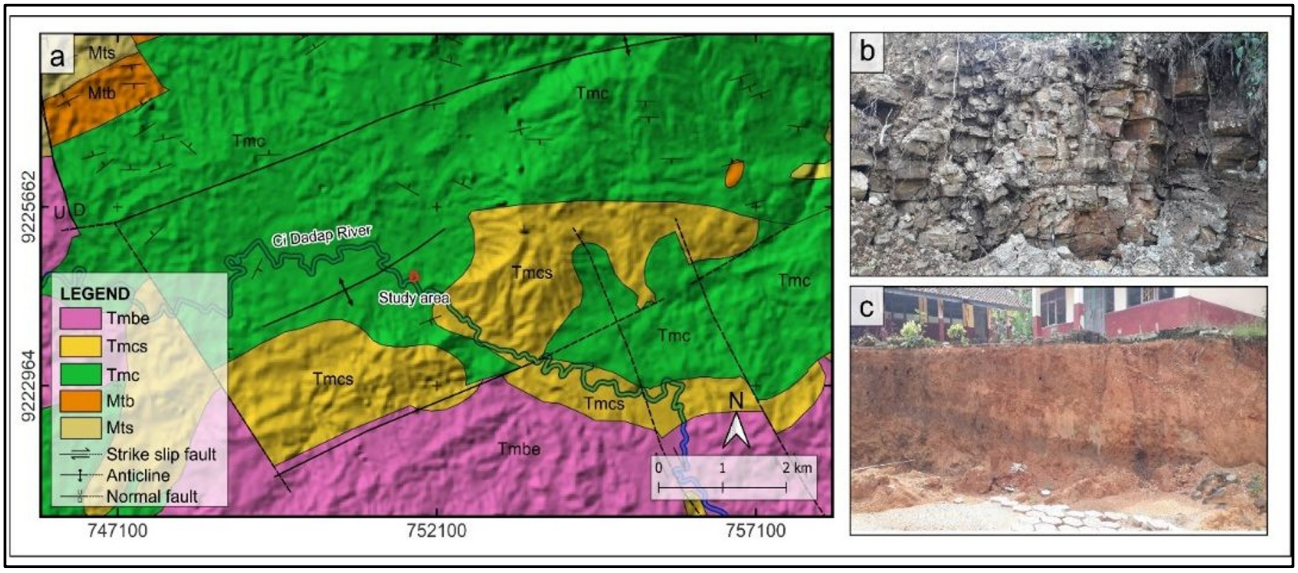

Fig. 1. The geological setting map of study area (a); Layers of sandstone and siltstone in toe of landslide (b); Soil profile displaying some remarkable horizons-- a light brown color in the upper layers and a dark brown color in the lower layers (c)

1.2 Rainfall

The ground in SDN Babakan Talang 01 started to rupture on Sunday, 18/02; the cracks were between 20 and 25 cm wide. The holes were quickly filled in with soil by locals. On Thursday, February 29, 2024, the ground began to massively slide as a result of the cracks' eventual extension and deepening. The cracks extend to 2-2.5 m by Monday, March 4, 2024. There was a definite circular pattern of landslides where some areas of the top ground collapsed about 3.5 and 4 meters.

The timing of the Rongga landslide on 4 March 2024 links with the very wet rainy season that had been ongoing since October 2023 with rainfall ranging between 40 to 80 mm per day in December, January and March (Fig. 2). In the week before the landslide rainfall intensity was the highest at 100 mm, while satellites reported total rainfall in the order of 3150 mm, 2050 mm, and 1500 mm according to IMERG [6], MERRA-2 [7], and GsMAP [8].

The ERT survey, done on May 23, 2024, a few weeks before, happened in a dry period. This rainfall data is important for assessing the water content in the surface and subsurface layers in the framework of the ERT analysis. The high total rainfall prior to the landslide, together with the start of the event in the afternoon after already extremely high daily rainfall, might have affected the moisture status and hydrological situation in the surrounding. Knowledge of these rainfall patterns and how they affect subsurface water dynamics is crucial because both the interpretation of ERT results and the evaluation of geological hazards related to landslides depend on this information in the case region.

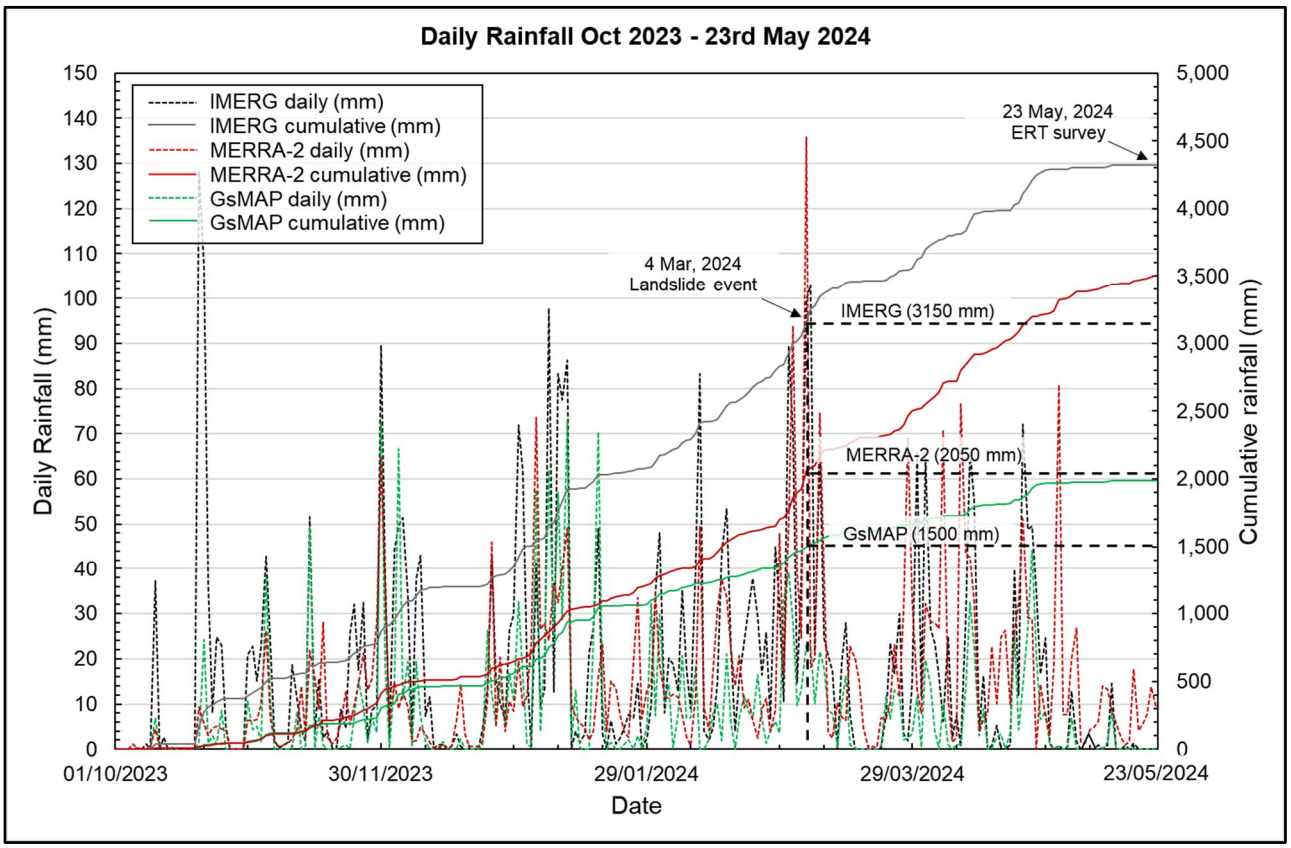

Fig. 2. This dataset is a compilation of daily and cumulative rainfall data from IMERG, MERRA-2, and GsMAP satellites showing the distribution of rainfall during the period October 2023 to May 23, 2024. The dash line represents daily rainfall, and the solid line summarizes rainfall accumulation over the period of the study area, offering how many days and how hard it rained.

2 Methodology

2.1 Electrical resistivity method (ERT)

In studying landslides, the selection of electrode configuration plays a role in the appropriateness of the resolution and the depth window to detect. One of the recommended configurations includes all Dipole-Dipole configurations that can give the target depth window of say 15 meters. This combination is applicable because of the balance between penetration depth and resolution. As such, there must be good horizontal structures and changes to show some slip surfaces and fractures. Electrode spacing constitutes another factor to include and, depending on the target, aims for the effective element. The following is the key formula for telling the apparent resistivity (ρ_a) in a dipole-dipole equation. The apparent resistivity (ρ_a) is expressed as:

$$\rho a = \frac{2\pi a(n+1)(n+2)\Delta V}{I} \quad (1)$$

where:

- a is the distance between electrodes,
- n is the possible number of electrodes spacings which the current dipole and the potential dipole could be correlated,
- ΔV is the potential difference being measured,
- I is the ground current injected into the ground.

The electrodes in a dipole-dipole configuration are placed similarly in a straight line. C_1 and C_2 are the two electrodes used to apply the current to the ground. We used a second pair of electrodes, named P_1 and P_2, to measure the voltage caused by the same current. As depicted in Fig. 3, the current electrodes C_1 and C_2 are spaced by a distance of. The potentials P_1 and P_2 are located at a half distance of the midpoint between C_1 and C_2, and with other half from the separation point, P_1 and P_2. It does this by measuring the potential difference between P_1 and P_2 which is affected by the current that is injected by C_1 and C_2, to the ground.

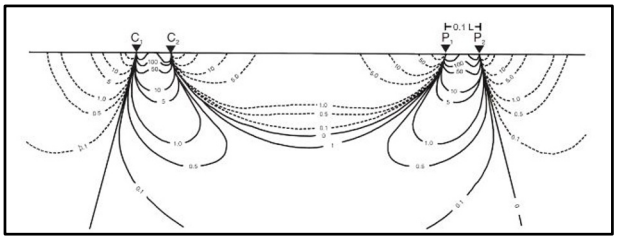

Fig. 3. Illustration of signal contribution sections for dipole-dipole configurations, the contours represent the contribution of different volume elements in the subsurface to the total potential difference measured between the potential electrodes P_1 and P_2. This setup enables precise measurement of the electric field perturbations created due to the injected current, and so it provides an exact function of the changes in the subsurface resistivity.

Table 1. The detail of ERT survey

Name of Tools	SuperSting with Swift R8
Configuration	Dipole-Dipole
Spacing (m)	3
Number of Electrodes	56
Max Depth Penetration (m)	84
Length of Line (m)	165
Number of Line	2

The optimal electrode spacing for a dipole-dipole ERT configuration to effectively detect features at a depth around 15 meters typically ranges between 2 to 5 meters. Three meters was chosen because that offers a balance between resolution and depth penetration. It allows for a reasonable level of detail while still being capable of reaching depths around 15 meters. Table. 1 provides detailed information on survey settings.

Generally, it is good to have those electrodes 2-5 meters apart to do a dipole-dipole ERT configuration that is best for 10-15meter depth features. Three meters is a good choice as it keeps the right balance between resolution and depth penetration. It provides a good amount of resolution and yet is capable of going to depths approaching 15 meters. Table. 1 gives an elaborate info as seen in the meanwhile in survey settings.

2.2 Waterpass, altimeter, and GPS

Orion 2LS Digital Waterpass Level (Fig. 4. a and b), Micro Altimeter Alpinel 0.5 m Barograph Correction (Fig. 4c), and Garmin GPSMAP (Fig. 4c) enhances data accuracy and dependability collected in geophysical surveys. Correct leveling of the surface is critical for having the electrodes at the correct location in ERT surveys to acquire optimal data. The accuracy of this digital level keeps the electrodes from falling out in the trough and registers very consistent data. An electronic sensor inside the Orion 2LS Digital Level Waterpass measures the tilt angle of the device. The black and white striped ruler is the target for the level's laser or optical system (Fig. 4b). The device is designed to detect the position of the stripes when a laser or optical signal is directed at the ruler, thereby identifying height differences or the tilt angle with respect to the ruler. This data is then digitally processed and output, enabling highly accurate leveling and alignment using the ruler location.

In addition, the Micro Altimeter Alpinel is distinct in the way it adjusts for changes in barometric pressure to offer precise (Fig. 4c). This accuracy is extremely important in correcting ERT resistivity surveys for topographic bias and thus increasing data accuracy. The control over topographical variations due to accurate altitude data assists in producing less variably subsurface resistivity models.

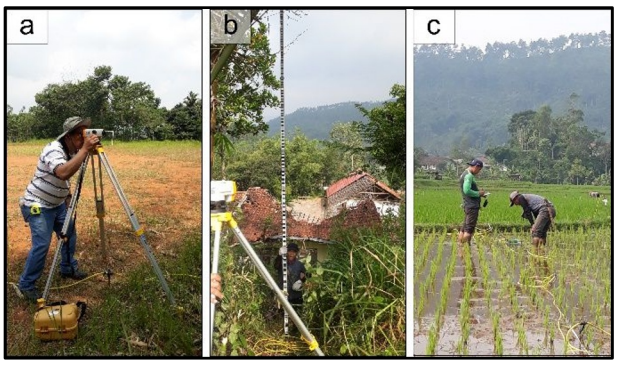

Fig. 4. a. Measuring distance and height to the black and white striped ruler which is the orion 2LS digital level waterpass **b.** The black and white striped rule, possibly a target for a level's laser or optical system **c.** Combination of micro altimeter alpinel and the garmin GPSMAP for correct altitude and gps navigation.

High-sensitivity GPS capabilities provide precise coordinates in the Garmin GPSMAP for each electrode position (Fig. 4c). This precision both helps in laying out the survey grid correctly, thus limiting positioning errors and enhancing the quality of the resistivity measurements as a result. In combination, however, these tools ensure that electrodes are placed correctly in all three dimensions, which greatly improves accuracy and repeatability of geophysical survey data.

The Orion 2LS Waterpass provides accurate horizontal leveling and the Micro Altimeter Alpinel compensates for any changes in elevation. Garmin GPS provides precise location information by combining latitude, longitude, and altitude. This is achieved by a combined application of these tools, which enables eliminating the most common positioning errors, where all electrodes are properly positioned relative to three dimensions. This setup allows for accurate and reliable data, a must for any valuable geophysical survey.

3 Results

The ERT (Electrical Resistivity Tomography) image provides a detailed subsurface cross-section of a location characterized by sediment and volcanic deposits, including sand, clay, and weathered volcanic soil. The resistivity values are color-coded, with blue representing low resistivity and red indicating high resistivity. In this image, key observations can be made regarding saturation

levels, potential sliding surfaces, and structural features such as grabens.

This ERT (Electrical Resistivity Tomography) image was obtained to represent the subsurface section of the study area consists of sedimentary and volcanic deposits of sand, clay and weathered volcanic soil. The subsurface condition is the result of resistivity values - blue is least resistive, red is most resistive. This detail allows for a number of observations on type of rock and soil, saturation level, potential sliding surfaces and structural elements such as grabens to be made.

3.1 The key feature

3.1.1 Saturation and gradient saturation

When the formation has a low resistivity, only blue and light blue can be seen, which is typical for clay or for sand saturated with water. However green into yellow areas which represent moderate resistivity imply the presence of more poorly saturated materials (likely sand or soil and varying moisture content). Red (high resistivity) and orange regions indicate dry materials such as dry sand or volcanic deposit (volcanic ash) or compacted, less porous sediments in case of (Figs. 5 and 6).

3.1.2 Sliding surface and graben

In marks of resistivity variability, it might expose some of potential sliding or slip surfaces. For example, the change from high resistivity (red/yellow) to lower resistivity (blue) might indicate a slip surface where saturated clay (blue) underlies less saturated material (yellow/red). Sudden changes in resistivity as well as notable slope (slope break) or gradients changes in the contour further indicate the possible sliding surfaces, especially in cases where the high resistivity material is sitting on the low resistivity zones. At the same time, a low structure in resistivity values is visible within the central part of the image, plunging downward and indicating the occurrence of a small-graben structure Fig. 6. Such things could be a simple graben - a trough or sunken block between rifts or between parallel faults, usually with the gravity-induced phenomenon of mass-wasting associated with landslides. The low resistivity areas (blue) that are suggested (assuming a lateral variability of this parameter in the subsurface) on the central lower part of the image, are most likely indicative of a graben filled with saturated materials probably induced by an extensional mechanism linked to the movement of the landslide. If that is what it is, then it may indicate a zone where the ground has dropped down, becoming a conduit for water to pool, pushing the sediments on the ground to start moving. The description of the ERT profile of Fig. 5 in three sections:

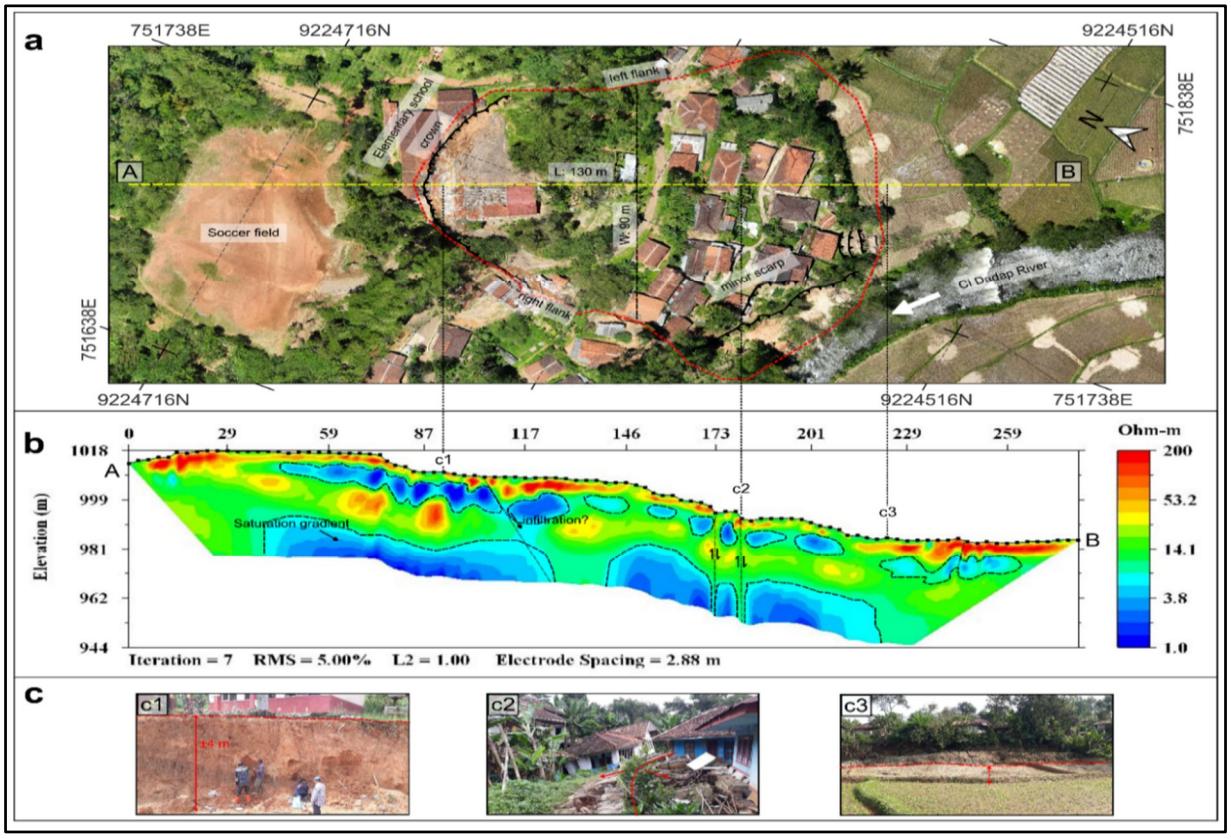

Fig. 5 An orthogonal aerial photograph of the Rongga landslide location (a); The red dashed line indicates the landslide-affected area, the black line denotes the scarp, and the Ci Dadap River converges at the foot of the slope (b); Electrical resistivity tomography (ERT) profile dipole-dipole configuration, ERT 2 lines with 3 meters electrodes separation/56 electrodes; An image of the crown landslide scarp with 4 meters drop (c1); A house twisted during landslide (c2); Bullging occuring at toe of landslide (view about 1m) of landslide (c3)

3.1.3 Fig. 5 left section (0-87 meters)

This section of the ERT profile shows high resistivity in near-surface layers (red/yellow colors) comprising dry or dense sediments or volcanic deposits. Deep background blue areas where these are shallow suggest increased moisture content in nearby clay layers or water-saturated sediments beneath. The potential slip surface is characterized by high resistivity (red/yellow) intersecting a low resistivity (blue) material which may be a geological interfacial zone of geological boundaries where various types of materials or moisture phases meet.

3.1.4 Fig. 5 middle section (87-201 meters)

The ERT profile shows a characteristic low resistivity zone (blue coloration) in this water bearing horizon. This zone indicates a graben-like structure or an area on which fluids (in this case, water) have pooled. The greener/yellower zones above this low resistivity zone correspond with less saturated materials. Based upon the boundary between these resistivity anomalies, potential sliding surfaces are inferred, indicating potential geological failure surfaces as a result of motion or deformation.

The base of the fault plane is estimated to be situated around 180 meters in the horizontal with a continuation up the vertical from approximately 999 meters to between 962 - 944 meters in elevation. This fault plane exhibits a strong vertical resistivity contrast, with high-resistivity on the right-left side colored in yellow or red, and low-resistivity (blue/green) in the middle.

3.1.5 Fig. 5 right section (201-259 meters)

Like the left section, the upper layers near the surface show high resistivity (red/yellow: dry sediments or volcanic deposits). Below texture these blue zones return and this shows more moisture or water-saturated sediments. Abrupt changes in resistivity indicate possible slip surfaces in the same manner as seeing things in the left view.

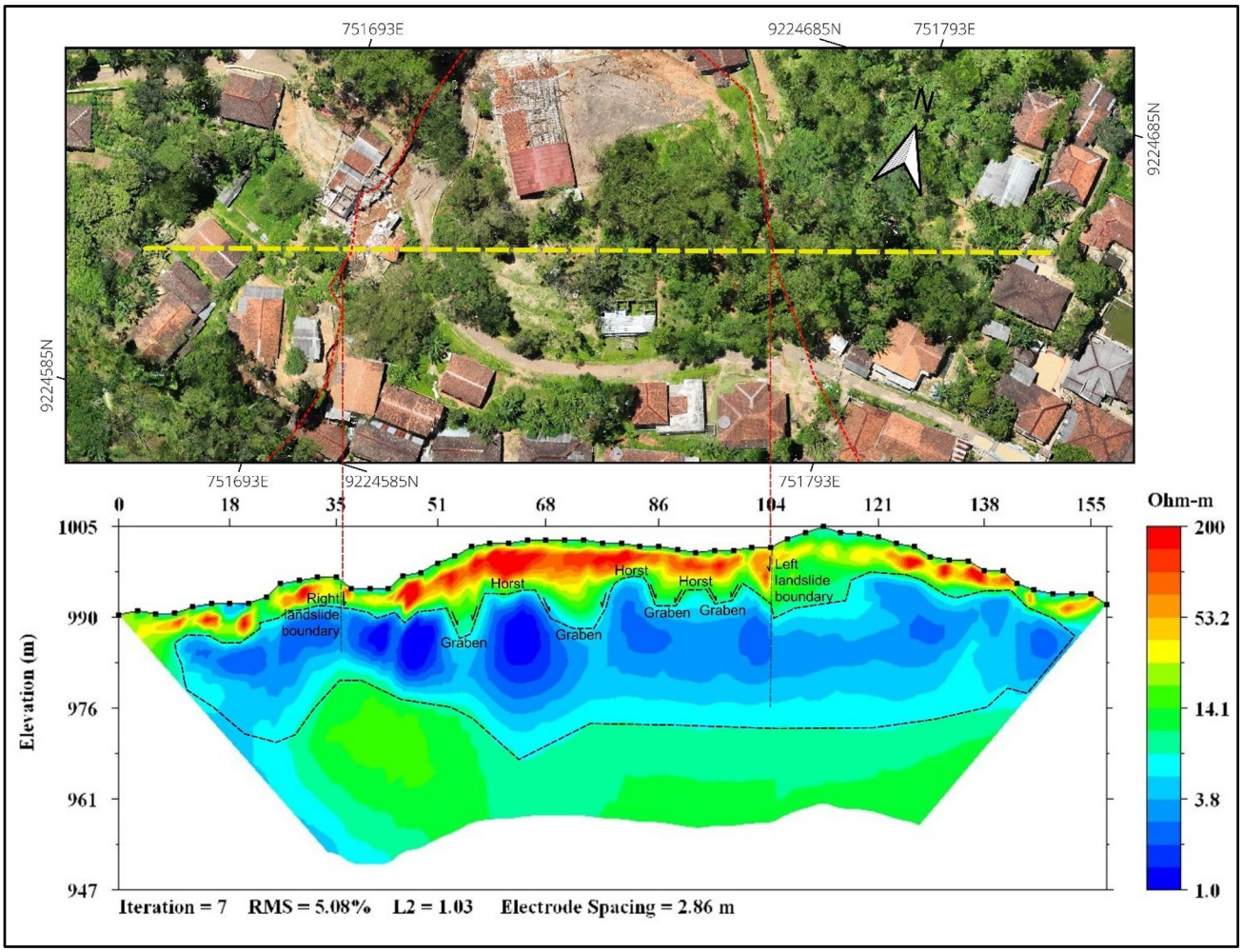

Fig. 6. Above: an orthogonal aerial photograph of the Rongga landslide location. The red dashed line indicates the landslide-affected area, bottom: electrical resistivity tomography (ERT) profile dipole-dipole configuration, ERT 2 lines with 3 meters electrodes separation 56 electrodes

4 Discussion

The Rongga landslides are primarily influenced by a combination of lithology, river erosion, and fault structures. First, the lithology of the area, which consists of interbedded sandstone, siltstone, and claystone, plays a significant role in landslide susceptibility. The impermeable nature of claystone layers prevents effective drainage, leading to increased pore water pressure in the soil and slope instability. This pressure build-up can cause the claystone to degrade, weakening the material and making it more prone to slope failure [9], [10] . As a result, the claystone often acts as a sliding plane, affecting overall stability, especially under high rainfall conditions that exacerbate drainage challenges [11], [12]. Furthermore, the interbedded nature of these rocks forms a complex system that interacts with surrounding geological features, thus heightening landslide risk.

Second, river erosion at the Cidadap River bank (Fig. 7), located near the base of the slope, has likely intensified landslide dynamics. Heavy rainfall in recent months has accelerated the erosion process, exposing weathered claystone along the riverbank [13], [14]. This exposure to weathering weakens the claystone, reducing its shear strength and directly contributing to riverbank failure. The loss of bank strength further destabilizes the slope, making it more susceptible to landslides. This combination of erosion and weathering amplifies the vulnerability of the Rongga landslide area to collapse.

Fig. 7. Failure at Cidadap River bank

Finally, Electrical Resistivity Tomography (ERT) results revealed the presence of a fault structure in the lower-middle region of the landslide area. This fault, indicated by the presence of joints measuring 20 to 50 cm wide as shown in Fig. 8, signifies tectonic influence in the area [15], [16]. The fault's formation is linked to an anticline with folded lithology-oriented southeast-northwest, suggesting that local tectonics contribute to the structural weaknesses in the slope. This fault structure amplifies the landslide risk, as it interacts with the surrounding hydrological and geological conditions, creating a dynamic and unstable environment prone to failure. Additionally, the fault plane's low resistivity readings on one side suggest variations in material composition, potentially indicating fluid pathways or differences in compaction and water content [17], [18]. This resistivity contrast is crucial for understanding subsurface dynamics, as it may affect groundwater flow and influence geological hazards.

Fig. 8. Intensive joint in study area

5 Conclusion

The findings emphasize the complex interplay between lithology, river erosion, and tectonic activity as primary triggers for the Rongga landslides. The impermeable claystone layers contribute to increased pore water pressure, compromising slope stability, while river erosion exacerbates slope degradation by weakening riverbank support. Additionally, the fault structure, with its well-defined resistivity contrast and vertical extent, highlights the influence of tectonic activity on landslide susceptibility in the area. This fault's significant resistive boundary implies a strong tectonic influence that warrants further investigation for potential seismic implications, which could affect infrastructure planning and hazard mitigation strategies.

Future research should focus on refining and validating the ERT data to further elucidate the subsurface conditions, particularly along the fault plane. Ground-truthing studies and high-resolution ERT surveys could provide more accurate data on the fault's behavior, while integrating other geophysical methods would offer a comprehensive understanding of subsurface dynamics. Additionally, collaborations with experts in structural geology, geotechnical engineering, and hazard assessment are essential to gain multidisciplinary insights into the implications of the fault and resistivity variations. By combining these research approaches, future studies can generate a holistic view of the study area, aiding in land use planning, infrastructure development, and hazard mitigation in tectonically active regions.

This integrated analysis, grounded in multidisciplinary research, will not only improve our understanding of the geological conditions and fault dynamics but also offer critical data for sustainable development and risk management in the area.

This research is funded by Rumah Program Kebencanaan Hidrometeorologi dan Iklim - Organisasi Riset Kebumian dan Maritim -Badan Riset dan Inovasi Nasional (BRIN), Indonesia for 2024. The authors would like to thank for supporting them for conducting this work.

References

1 A. Perrone, V. Lapenna, and S. Piscitelli, Electrical resistivity tomography technique for landslide investigation: A review. Earth-Science Rev., **135**, 65–82, (2014)

2 M. Sun, J. Liu, J. Ou, R. Liu, and L. Zhu, Electrical Resistivity Tomography (ERT) Investigation for Landslides: Case Study in the Hunan Province, China. Appl. Sci., **14**(7), (2024)

3 C. Ling, Q. Xu, Q. Zhang, J. Ran, and H. Lv, Application of electrical resistivity tomography for investigating the internal structure of a translational landslide and characterizing its groundwater circulation (Kualiangzi landslide, Southwest China). J. Appl. Geophys., **131**, 154–162, (2016)

4 M. H. Z. Putra, R. D. Kartiko, P. Soemantidiredja, I. A. Sadisun, and A. Tohari, Pengaruh Zona Jenuh Air Terhadap Kestabilan Lereng Di Weninggalih, Kabupaten Bandung Barat. Ris. Geol. dan Pertamb., **30**(1), 119, (2020)

5 M. Koesmono, Kusnama, and N. Suwarna, Geological Map of The Sindangbarang and Bandarwaru Quadrangles, Jawa. 2nd Edition. Geological Research and Development Centre, (1996).

6 G. J. Huffman, E. F. Stocker, D. T. Bolvin, E. J. Nelkin, and J. Tan, GPM IMERG Final Precipitation L3 1 day 0.1 degree x 0.1 degree V07, Edited by Andrey Savtchenko, Greenbelt, MD, Goddard Earth Sciences Data and Information Services Center (GES DISC), (2023). [Online]. Available: https://disc.gsfc.nasa.govuni/datasets/GPM_3IMERGDF_07/summary. [Accessed: 23-Aug-2024].

7 GMAO, Global Modeling and Assimilation Office. inst3_3d_asm_Cp: MERRA-2 3D IAU State, Meteorology Instantaneous 3-hourly (p-coord, 0.625x0.5L42), version 5.12.4, Greenbelt, MD, USA: Goddard Space Flight Center Distributed Active Archive Center (GSFC DAAC), (2015). [Online]. Available: https://gmao.gsfc.nasa.gov/reanalysis/merra-2/citing_MERRA-2/. [Accessed: 23-Aug-2024].

8 T. Kubota *et al.*, Global Satellite Mapping of Precipitation (GSMaP) products in the GPM era, Satellite precipitation measurement, Springer, (2020). [Online]. Available: https://sharaku.eorc.jaxa.jp/GSMaP/. [Accessed: 23-Aug-2024].

9 P. K. Singh, K. K. Singh, and T. N. Singh, Slope failure in stratified rocks: a case from NE Himalaya, India, *Landslides*, **14**(4), 1319–1331, (2017)

10 A. W. Skempton, Residual strength of clays in landslides, folded strata and the laboratory, *Geotechnique*, **35**(1), 3–18, (1985)

11 A. Cevasco, G. Pepe, and P. Brandolini, The influences of geological and land use settings on shallow landslides triggered by an intense rainfall event in a coastal terraced environment, Bull. Eng. Geol. Environ., **73**(3), 859–875, (2014)

12 L. C. Nguyen, P. Van Tien, and T. N. Do, Deep-seated rainfall-induced landslides on a new expressway: a case study in Vietnam, Landslides, **7**(2), 395–407, (2020)

13 T. R. Martha, P. Roy, K. B. Govindharaj, K. V. Kumar, P. G. Diwakar, and V. K. Dadhwal, Landslides triggered by the June 2013 extreme rainfall event in parts of Uttarakhand state, India, Landslides, **12**(1), 135–146, (2015)

14 S. C. Chen, H. Ter Chou, S. C. Chen, C. H. Wu, and B. S. Lin, Characteristics of rainfall-induced landslides in Miocene formations: A case study of the Shenmu watershed, Central Taiwan, Eng. Geol., **169**, 133–146, (2014)

15 G. Samodra, M. F. Ramadhan, J. Sartohadi, M. A. Setiawan, N. Christanto, and A. Sukmawijaya, Characterization of displacement and internal structure of landslides from multitemporal UAV and ERT imaging, Landslides, **17**(10), 2455–2468, (2020)

16 A. Viero, A. Galgaro, G. Morelli, A. Breda, and R. G. Francese, Investigations on the structural setting of a landslide-prone slope by means of three-dimensional electrical resistivity tomography, Nat. Hazards, **78**(2), 1369–1385, (2015)

17 J. Luhn, M. J. Stumvoll-Schmaltz, A. F. Orozco, and T. Glade, Internal structure of an active landslide based on ERT and DP data: New insights from the Hofermühle landslide observatory in Lower Austria, Geomorphology, **441** (2023)

18 M. T. Riaz, M. Basharat, K. S. Ahmed, Y. Sirfraz, A. Shahzad, and N. A. Shah, Failure mechanism of a massive fault–controlled rainfall–triggered landslide in northern Pakistan, Landslides, **21**(11), 2741–2767, (2024)